



UNIVERSITY OF LEEDS

This is a repository copy of *Thermal-physical properties of nanoparticle-seeded nitrate molten salts*.

White Rose Research Online URL for this paper:  
<http://eprints.whiterose.ac.uk/127822/>

Version: Accepted Version

---

**Article:**

Awad, A, Navarro, H, Ding, Y et al. (1 more author) (2018) Thermal-physical properties of nanoparticle-seeded nitrate molten salts. *Renewable Energy*, 120. pp. 275-288. ISSN 0960-1481

<https://doi.org/10.1016/j.renene.2017.12.026>

---

(c) 2017, Elsevier Ltd. This manuscript version is made available under the CC BY-NC-ND 4.0 license <https://creativecommons.org/licenses/by-nc-nd/4.0/>

**Reuse**

This article is distributed under the terms of the Creative Commons Attribution-NonCommercial-NoDerivs (CC BY-NC-ND) licence. This licence only allows you to download this work and share it with others as long as you credit the authors, but you can't change the article in any way or use it commercially. More information and the full terms of the licence here: <https://creativecommons.org/licenses/>

**Takedown**

If you consider content in White Rose Research Online to be in breach of UK law, please notify us by emailing [eprints@whiterose.ac.uk](mailto:eprints@whiterose.ac.uk) including the URL of the record and the reason for the withdrawal request.



[eprints@whiterose.ac.uk](mailto:eprints@whiterose.ac.uk)  
<https://eprints.whiterose.ac.uk/>

Energy

Elsevier Editorial System(tm) for Renewable

Manuscript Draft

Manuscript Number:

Title: Thermal-physical properties of nanoparticle-seeded nitrate molten salts

Article Type: VSI: Nanofluids & Renewable

Keywords: nanofluid, nitrate salt, specific heat capacity, latent heat, thermal energy storage, thermal diffusivity.

Corresponding Author: Professor Dongsheng Wen,

Corresponding Author's Institution: University of Leeds

First Author: Afrah Awad

Order of Authors: Afrah Awad; Helena Navarro; Yulong Ding; Dongsheng Wen

### Highlights

- Three types of nanoparticle were dispersed into two different types of solar salts.
- Nanosalts show enhanced thermal diffusivity/conductivity, sensible heat and latent heat.
- 0.5 wt. %  $\text{Fe}_2\text{O}_3$ -nanosalt increased thermal diffusivity of solar salt up to 50%.
- 14.5 % enhancement of the latent heat of solar salt was found for  $\text{KNO}_3$ .
- 5.3 % enhancement of the total storage capacity was found at  $155\text{ }^\circ\text{C} < T < 435\text{ }^\circ\text{C}$ .

# 1 Thermal-physical properties of nanoparticle-seeded nitrate molten salts

2 Afrah Awad<sup>1</sup>, Helena Navarro<sup>2</sup>, Yulong Ding<sup>2</sup>, Dongsheng Wen<sup>3,1\*</sup>

3 <sup>1</sup>School of Chemical and Process Engineering, University of Leeds, UK

4 <sup>2</sup>School of Chemical Engineering, University of Birmingham, Birmingham, UK

5 <sup>3</sup>School of Aeronautic Science and Engineering, Beihang University, China

6 Email: [d.wen@leeds.ac.uk](mailto:d.wen@leeds.ac.uk)

7

8

## 9 Abstract

10 Molten salts have been used extensively as energy storing materials, however, their  
11 thermophysical properties, such as specific heat capacity and thermal conductivity  
12 have limited their applications. In this study, potassium nitrate and sodium–  
13 potassium nitrate (NaNO<sub>3</sub>:KNO<sub>3</sub> with 60:40 molar ratio) are used as the base salts  
14 with different types of nanoparticles, which are iron oxide (Fe<sub>2</sub>O<sub>3</sub>), titanium dioxide  
15 (TiO<sub>2</sub>) and copper oxide (CuO) over a wide range of temperatures up to 500 °C.  
16 Laser flash analysis is used to measure thermal diffusivity and dynamic scanning  
17 calorimeter for specific heat (latent heat and melting temperature) of the molten salts  
18 and nanosalts. The addition of Fe<sub>2</sub>O<sub>3</sub> into sodium–potassium nitrate salt increases  
19 thermal diffusivity up to 50%. Moreover, the highest increase in the latent heat  
20 reaches 14.45% at 1 wt. % CuO-binary nitrate salt. In addition, the total thermal  
21 energy storage of nanosalt increases up to 6% including both of sensible and latent  
22 heat. The formation of the interface layer between nanoparticles and salts could be  
23 the reason behind this enhancement in sensible and latent heats. The surface area  
24 of the nanosalt measured by scanning electron microscopy showed a heterogeneous  
25 dispersion of nanoparticles in the nanosalt samples, including agglomerated areas  
26 that could be sometimes responsible for the degradation of the sensible or latent  
27 heats.

28

29 **Keywords:** nanofluid, nitrate salt, specific heat capacity, latent heat, thermal energy  
30 storage, thermal diffusivity.

31

32

### 33 **1. Introduction**

34 Solar energy is a promising renewable energy source for our energy future,  
35 (Thirugnanasambandam et al., 2010), but can be only used during the daylight. An  
36 integration with a storage system must be done to ensure the reliability and  
37 availability of the system. Solar energy can be stored in three different forms as  
38 sensible heat, latent heat or in thermochemical form. Thermochemical reactions  
39 could provide higher energy storage density but it needs very complex systems to  
40 control these reactions.

41 Molten salt is generally used to store energy in sensible/latent forms. For example,  
42 most of the concentrated solar thermal power plants have been integrated with  
43 sensible storage tanks, i.e., one hot tank and one cold tank to store the energy up to  
44 390 °C. Considering that the melting temperature of solar salt (NaNO<sub>3</sub>: KNO<sub>3</sub> with  
45 60:40 molar ratios) is 232 °C and for potassium nitrate (KNO<sub>3</sub>) is around 334 °C, any  
46 of them is a good choice for sensible heat storage (Chieruzzi et al., 2013, Chieruzzi  
47 et al., 2015). Another advantage of molten salt is its higher energy density due to its  
48 change phase with an approximately constant temperature giving a higher latent  
49 heat, e.g. the latent heat of KNO<sub>3</sub> is around 91.61 KJ/kg and solar salt is 110.01  
50 KJ/kg (Chieruzzi et al., 2013, Chieruzzi et al., 2015a). The use of molten salt as a  
51 phase change material (PCM) for solar thermal applications has been investigated  
52 by many researchers such as (Feldhoff et al., 2012, Laing et al., 2009, Pflieger et al.,  
53 2015, Luo et al. 2017). However, their limited thermo-physical properties such as  
54 thermal conductivity,  $k$ , (in the range from 0.1-0.6 W/m.°K (Kong et al., 2014)) and  
55 specific heat capacity ( $cp$ ) have prevented its wide applications.

56 Nanoparticles have been recently proposed to solve the problem of low  $cp/k$  values  
57 of the nitrate molten salt. Many work have shown that dispersing nanoparticles to a  
58 base salt (here called nano-salt) at low concentrations could increase the  $cp$  value,  
59 but the results are inconclusive. There are different types of nitrate molten salt  
60 studied, including single nitrate salt, binary or ternary nitrate salt, which are briefly  
61 reviewed below. Chieruzzi et al. (2015b) studied the effect of silica, alumina and  
62 hybrid silica-alumina nanoparticles on single nitrate salt (KNO<sub>3</sub>) salt. On the other  
63 hand, Lasfargues et al. (2015) studied the effect of dispersing CuO and TiO<sub>2</sub>  
64 nanoparticles on a binary nitrate (solar salt) and showed that the maximum increase

65 in cp was 10.48% at 440 °C for 0.1 wt. % CuO-solar salt. Moreover, different types of  
66 nanoparticles, with different concentrations and size have been dispersed into a  
67 binary nitrate solar salt to improve the cp of nanosalt (Andreu-Cabedo et al., 2014,  
68 Chieruzzi et al., 2013, Dudda and Shin, 2013, Lu and Huang, 2013, Riazi et al.,  
69 2016, Schuller et al., 2015, Luo et al., 2017). Others investigated the effect of  
70 dispersing silica, multi-walled carbon nanotubes, hybrid silica-alumina, Mica, gold  
71 and alumina nanoparticles into nitrate solar salt (Andreu-Cabedo et al., 2014,  
72 Chieruzzi et al., 2013, Dudda and Shin, 2013, Jung and Banerjee, 2011, Lu and  
73 Huang, 2013, Niu et al., 2014, Riazi et al., 2016, Schuller et al., 2015). Some of their  
74 results showed a higher increase in cp of nanosalt, which was dependent on the  
75 types, sizes, and concentrations of nanoparticles used. Others showed different  
76 results. This increase or decrease in the literature for the cp values of the nanosalt  
77 samples could be related to different sources of the materials used either molten salt  
78 (with different purities and suppliers) or the nanoparticles (different sources of the  
79 purchased companies or supplied by the researchers themselves). In addition,  
80 different preparation protocols and measurement conditions could also be the  
81 reasons. In order to explain the enhancement in cp of nanosalt samples, the  
82 literature indicated that interfaces were formed between the molten salt and  
83 nanoparticles (Riazi et al., 2016, Luo et al., 2017). Another explanation is the  
84 increment in the thermal resistance due to the effect of nanoparticles, which own  
85 higher surface areas. However, the simple mixing model, which relays on higher cp  
86 of nanoparticles itself in most of the cases, is not applicable to the nanosalt case as  
87 the cp of the nanoparticle is still less than cp of the molten salt.

88 Furthermore, extensive studies have been conducted on the enhancement of  
89 thermal conductivity by adding nanoparticles, and a term 'nanofluid' was coined  
90 (Buongiorno et al., 2009, Chol, 1995), However, the base-fluids tested were water,  
91 mineral oils and polyalphaolefins lubricant (PAO). Only very limited work has been  
92 conducted on molten salts. For instance, thermal conductivity (k) of binary nitrate salt  
93 with Al<sub>2</sub>O<sub>3</sub> nanoparticles was measured using the laser flash analysis (LFA), which  
94 showed that adding nanoparticle decreased k in a temperature range between 65<sup>0</sup>  
95 C- 145<sup>0</sup> C (Schuller et al., 2012). Additionally, Myers et al. (2016) measured the  
96 thermal conductivity of the solid phase for three different types of nitrate molten salts  
97 (i.e., potassium nitrate, sodium nitrate, and the potassium–sodium nitrate eutectic

98 (54 weight percent potassium nitrate) with copper oxide (CuO) nanoparticles. Their  
99 results showed an increment in thermal conductivity of the nanosalt, due to the  
100 formation of nanostructures between the nanoparticles and the molten salt. On the  
101 other hand, Shin (2011) studied the thermal conductivity when dispersing silica  
102 nanoparticles (1 wt.%) in carbonate salt of lithium: potassium carbonate salt ( $\text{Li}_2\text{CO}_3$ :  
103  $\text{K}_2\text{CO}_3$  with 62:38 by molar ratio) up to 300 °C. The results showed an enhancement  
104 in k by 37%-47%, and it was believed that smaller size of nanoparticles increment  
105 the interfacial thermal resistances resulted in a k decrease. They also indicated that  
106 none of the two models, The Hamilton\_Crosser and Maxwell\_Garnett models could  
107 predict the enhancement correctly.

108 It shall be noted that both  $c_p$  and k, or thermal diffusivities, values are needed to  
109 assess the performance of a molten salt, including the storage capacity and  
110 charging/discharging behaviour. However, none of the work reported so far have  
111 reported these properties in one study. From the k side, none of the previous  
112 studies shows the effect of different nanoparticles on thermal conductivity over a  
113 wide range of temperatures up to 500 °C by taking into consideration of both solid  
114 phase and liquid phases.

115

116 In this work, we investigate experimentally the thermal-physical properties (k,  $c_p$ ) of  
117 nanosalts to reveal the performance of nanoparticles. Different concentrations (0.5  
118 wt. %, 1 wt. % and 1.5 wt. %) of  $\text{Fe}_2\text{O}_3$ , CuO and  $\text{TiO}_2$  on single salt ( $\text{KNO}_3$ ) and  
119 binary solar salt are studied. The thermal conductivity is determined by a laser flash  
120 analysis device; the thermal diffusivity data, including both solid and liquid phases,  
121 are measured up to 500 °C. The  $c_p$ , melting temperature, and heat of fusion are  
122 measured by a dynamic scanning calorimeter (DSC) device. In addition, material  
123 characterization is also reported by the scanning microscopy (SEM) and the DLS of  
124 the nanoparticles size.

125

## 126 **2. Experiments**

### 127 **2.1 Material**

128 The base material used for this study is nitrate molten salt. Sodium nitrate ( $\text{NaNO}_3$ )  
129 was purchased from (FISHER, Loughborough, UK) with 98% purity and potassium

130 nitrate ( $\text{KNO}_3$ ) from (SIGA-ALDRICH, Suffolk, UK) with 98% purity. The additive  
131 materials were copper oxide ( $\text{CuO}$ ) nanoparticles (<50 nm particle size) purchased  
132 from Sigma-Aldrich Company, and iron oxide ( $\text{Fe}_2\text{O}_3$ ) nanoparticles (20–40 nm  
133 particle size) purchased from (iolitec-USA company). The commercial titanium  
134 dioxide ( $\text{TiO}_2$ ) nanoparticles purchased from nanostructured & amorphous materials  
135 Inc., with purity of 99.8% and an average diameter of 50 nm.

136 The samples were prepared by the two-step method. Birefly, the nanoparticles were  
137 firstly mixed with molten salt and distilled water (30 ml), followed by a sonication  
138 process to ensure a good dispersion of nanoparticles within the sample. Then  
139 evaporation of water from the sample was conducted on a hot plate at a temperature  
140 around  $150\text{ }^\circ\text{C}$  until the water was fully evaporated from the samples.

141

## 142 **2.2 Measurement**

### 143 **i) Differential scanning calorimetry (DSC)**

144 Specific heat capacity tests were performed on a Mettler Toledo DSC (DSC1, Mettler  
145 Toledo, Leicester, UK) for single salt, binary salt, nanoparticles ( $\text{Fe}_2\text{O}_3$ ,  $\text{CuO}$ , and  
146  $\text{TiO}_2$ ) and nanosalt (with different concentrations of nanoparticles, e.g. 0.5 wt. %, 1  
147 wt. % and 1.5 wt. %), as well as the latent heat, and  $T_{\text{melting}}$  of molten salt and  
148 nanosalt. The sample was placed in the crucible made of platinum, sample's weight  
149 was in the range of 30 mg to 35 mg excluding the weight of the crucible in order to  
150 have enough materials to fill the pan but not too much to cause the overflow issue  
151 during the measurements. The sample was measured by an Ultra-microbalance  
152 Mettler Toledo balance. Sapphire was used as a standard material with known  
153 specific heat capacity values in the range of temperatures of the experiments. The  
154 heating method used was modelled at a rate of  $150\text{ }^\circ\text{C}$  for 10 min, ramped from  $150\text{ }^\circ\text{C}$   
155  $^\circ\text{C}$  to  $450\text{ }^\circ\text{C}$  at a rate of  $10\text{ }^\circ\text{C}/\text{min}$ , then maintained isothermally for 10 min at  $450\text{ }^\circ\text{C}$   
156 and finally cooled down from  $450\text{ }^\circ\text{C}$  to  $150\text{ }^\circ\text{C}$  at  $-40\text{ }^\circ\text{C}/\text{min}$ . It shall be noted that  
157 the maximum temperature in case of  $\text{KNO}_3$  base material is less than  $400\text{ }^\circ\text{C}$ .

158

### 159 **ii) Laser flash analysis (LFA)**



160 Laser flash analysis (LFA) device was implemented to measure thermal diffusivity of  
161 the sample. In the LFA measurement, the diffusivity was determined by heating the  
162 front face of the sample by a laser with simultaneous record of the temperature  
163 profile on the rear face

164 Three layers model is used in a LFA measurement. The sample is the layer with  
165 unknown diffusivity and the other two layers represent the samples' holder and the  
166 crucible lid with known properties, as shown in Figure (1). The elegance of the  
167 method lies in the fact that the troublesome measurement of the absolute quantity of  
168 laser energy absorbed by the sample and of the resulting absolute temperature  
169 increase is replaced with a more accurate and direct measurement of time and  
170 relative temperature increase.

171 In order to calculate the thermal conductivity of the samples, the values of density  
172 and the specific heat capacity are needed, and  $k$  can be calculated as shown in the  
173 Equation (1).

$$174 \quad k = c_p \times \rho \times a \quad (1)$$

175 where  $k$  is thermal conductivity  $W/m \cdot ^\circ K$ ,  $c_p$  is specific heat capacity  $J/kg \cdot ^\circ K$   
176 (measured in the DSC device),  $\rho$  is density in  $kg/m^3$  and  $a$ , is thermal diffusivity  $m^2/s$ .  
177 According to Janz et al. (1972), the density of binary nitrate solar salt can be  
178 calculated as a function of temperature depending on the Equation (2)

$$179 \quad \rho = 2064.31 - (4.76248 \times 10^{-4} \times T^2) - (3.36495 \times 10^{-7} \times T^3) \quad (2)$$

180 For nanosalt Equation (3) has been used by (Vajjha et al., 2009):

$$181 \quad \rho_{\text{nanosalt}} = (\varphi_{np} \times \rho_{np}) + ((1 - \varphi_{np}) \times \rho_{\text{salt}}) \quad (3)$$

182 where  $\varphi_{np}$  is concentration of nanoparticles,  $\rho_{\text{nanosalt}}$ ,  $\rho_{np}$  and  $\rho_{\text{salt}}$  are the density of  
183 nanosalt, nanoparticles and solar salt, respectively.

184

### 185 **iii) Scanning electron microscopy**

186 Morphology of the samples is performed by a scanning electron microscopy (Hitachi  
187 SU8230, SEM) device. SEM was used to show the surface morphology of molten

188 salt without and with nanoparticles. The samples were in powder form and their  
189 morphology before and after repeatable thermal cycles were studied.

#### 190 **iv) Dynamic light scattering**

191 Dynamic light scattering (Malvern Zetasizer ZS, DLS) was used to measure the size  
192 of nanoparticles in this work. Nanoparticles were dispersed in distilled water and  
193 then measured in DLS where the intensity vs particles size was obtained. Three  
194 different samples of three different nanoparticles ( $\text{Fe}_2\text{O}_3$ ,  $\text{CuO}$ , and  $\text{TiO}_2$ ) used in this  
195 work mixed with distilled water and sonicate before testing in the DLS device. We did  
196 not use any type of surfactant to stabilise the nanofluid, and as nanoparticles might  
197 have suffered from agglomeration, leading to a large particle size, shown in Figure  
198 (12).

199

### 200 **3. Results and discussions**

#### 201 **3.1 Specific heat capacity ( $c_p$ )**

202 The  $c_p$  results showed that adding nanoparticles to any of the nitrate molten salt  
203 used in the experiments (either single salt ( $\text{KNO}_3$ ) or binary salt (60  $\text{NaNO}_3$ :40  
204  $\text{KNO}_3$ )) had either a positive or negative effect, depending on many factors such as  
205 concentration, size or type of the nanoparticles used.

206 Figures (2-3) indicate that nanoparticles significantly affect the specific heat capacity  
207 of nanosalt. For solid phase results, 1.5 wt. % samples have larger increments in  $c_p$   
208 of nano-binary salt. In a similar study by using silica nanoparticles, Chieruzzi et al.  
209 (2013) who reported that 1 wt. % silica-nanosalt had higher  $c_p$  value than 0.5 wt. %  
210 or 1.5 wt.%. The slight difference might be due to the fact that different types of  
211 nanoparticles could behave differently with solar salt as well the differences in the  
212 preparation procedure between ours and the work of Chieruzzi et al. (2013).  
213 Chieruzzi et al. (2013) used an ultrasonic bath for 100 minutes and evaporated the  
214 water at  $200\text{ }^\circ\text{C}$ , while in ours, a probe sonicator was used with  $150\text{ }^\circ\text{C}$  to evaporate  
215 the water. The results of single salt,  $\text{KNO}_3$ , are highly dependent on the type of  
216 nanoparticles used, which is similar to what concluded by Chieruzzi et al. (2015a).

217 Figure (3) shows the dispersion of nanoparticles in  $\text{KNO}_3$  or binary salt increases the  
218 specific heat capacity of nanosalt at high temperature. However, this increase

219 depends on the type of the base material, concentrations and type of nanoparticles.  
 220 Mostly, TiO<sub>2</sub>-nanosalt shows a decrease in the  $c_p$  of nano-binary salt, as shown in  
 221 Table (3). In contrast, Lasfargues et al. (2015) indicated a positive effect of TiO<sub>2</sub>-  
 222 nanosalt and CuO-nanosalt. This difference could be due to different preparation  
 223 methods. For single salt case, Table (4) demonstrates that in most cases,  $c_p$   
 224 increases with the concentrations of nanoparticles. According to Chieruzzi et al.  
 225 (2015a), 1 wt.% of silica-KNO<sub>3</sub> salt has higher  $c_p$  than KNO<sub>3</sub> while 1 wt.% of alumina-  
 226 KNO<sub>3</sub> salt has lower  $c_p$  than KNO<sub>3</sub>. This is similar to the results we got for 1 wt. %  
 227 nano-KNO<sub>3</sub> however, Chieruzzi et al. (2015a) did not study the effect of another  
 228 concentration (0.5 wt.%). The increment of  $c_p$  of nanosalt in solid phase is slightly  
 229 higher than that of liquid phase especially for the case of solar salt as the base  
 230 material, which is in agreement to Chieruzzi et al. (2017).

231 From Tables (1-4), Fe<sub>2</sub>O<sub>3</sub> nanoparticles seem to be a good option to increase the  $c_p$   
 232 of the solid/liquid phase of the base material (either binary solar salt or single KNO<sub>3</sub>  
 233 salt) followed by CuO nanoparticles. TiO<sub>2</sub> nanoparticle gives a very small  
 234 enhancement in  $c_p$  of nanosalt or in most of the cases it decreases the  $c_p$  value.

235 There are some models used to predict the improvement in the  $c_p$  when  
 236 nanoparticles are added and these models are mentioned by many researchers for  
 237 example Seo and Shin (2014). The classical model of the effective specific heat can  
 238 be given by Equation (4)

$$239 \quad c_{p,nf} = \frac{\rho_{np} \phi_{np} c_{p,np} + \rho_f \phi_f c_{p,f}}{\rho_{np} \phi_{np} + \rho_f \phi_f} \quad (4)$$

240 where  $c_{p,nf}$ ,  $c_{p,np}$  and  $c_{p,f}$  represent  $c_p$  of nanosalt, nanoparticle, and salt.  $\phi_{np}$  and  $\phi_f$   
 241 are the volume fraction of nanoparticles and salt.  $\rho_{np}$  and  $\rho_f$  are the density of  
 242 nanoparticle and salt respectively. However, this model would not show any  
 243 enhancement in  $c_p$  unlike the most of the experimental results. This discrepancy is  
 244 due to the lower value of  $c_p$  of nanoparticles comparing to the salt. For instance,  $c_p$  of  
 245 Fe<sub>2</sub>O<sub>3</sub> nanoparticle is smaller than that of a molten salt. Even the fact that  $c_p$  of  
 246 nanoparticles is larger, e.g.  $c_p$  of Fe<sub>2</sub>O<sub>3</sub> around (0.9 J/g. °C), which is slightly higher  
 247 than its bulk material (0.84 J/g. °C) in the range of (150 °C – 450 °C) as indicated by  
 248 Snow et al. (2010). For more emphasis, we measured the  $c_p$  of all nanoparticles  
 249 used for the current experiments. In this experiments,  $c_p$  of Fe<sub>2</sub>O<sub>3</sub> equals to 0.9 J/g

250 C,  $c_p$  of CuO equals to 0.59 J/(g C) and  $c_p$  of TiO<sub>2</sub> is 1.06 J/g C. Furthermore, Zhou  
 251 and Wang (2003) referred that  $c_p$  of bulk CuO was 0.54 J/ (g. °C). While the  $c_p$  of  
 252 CuO nanoparticles measured in the current experiment equals to 0.59 J/ (g. °C)  
 253 which is slightly higher than  $c_p$  of its bulk material. However,  $c_p$  values of Fe<sub>2</sub>O<sub>3</sub> /  
 254 CuO/ TiO<sub>2</sub> nanoparticles are still lower than that of a molten salt. This indicates that  
 255 the increases in  $c_p$  are not due to the nanoparticle effect. Therefore, the classical  
 256 model cannot predict the enhancement in  $c_p$  of nanosalt where the  $c_p$  of molten salt  
 257 is larger than that of the nanoparticles used in the respective work. Therefore, this  
 258 model needs to expand and include the other factors such as the interfacial area  
 259 formed at the surface of the nanoparticle and the molten salt or other forces between  
 260 nanoparticles and so on.

261 Moreover, higher surface area owned by nanoparticles causes an increase in the  
 262 thermal resistance between nanoparticles and the molecules of the molten salt,  
 263 resulting in a rise in the interfacial interaction between them, which could increase  
 264 the  $c_p$  of a nanosalt. Additionally, during the preparation of the nanosalt sample and  
 265 due to the sonication and evaporation stages, molten salt molecules could form a  
 266 compressed layer on the surface of nanoparticles. These interfacial layers could  
 267 have different properties to the base material alone. Furthermore, these layers could  
 268 higher  $c_p$ , which may lead to increase the  $c_p$  of nanosalt according to the Equation  
 269 (5)

$$270 \quad c_{p,nf} = \frac{\rho_{np} \phi_{np} c_{p,np} + \rho_c \phi_c c_{p,c} + \rho_f \phi_f c_{p,f}}{\rho_{np} \phi_{np} + \rho_c \phi_c + \rho_f \phi_f} \quad (5)$$

271 where  $c_{p,c}$ ,  $\phi_c$  and  $\rho_c$  represent  $c_p$ , volume fraction, and density of compressed layer  
 272 (interfacial layer), respectively.

273 In addition, the mass fraction of these layers depends on size and concentrations of  
 274 nanoparticles. It is assumed that the  $c_p$  of an interfacial layer has a significant effect  
 275 on the overall  $c_p$  of nanosalt when there is no agglomeration of nanoparticles. For  
 276 instance, an assumed value of  $c_p=6.2$  J/g.°K (of the interfacial layer) would predict  
 277 the experimental well. Other possible reasons that could have the higher effect on  
 278 the  $c_p$  of the nanosalt are the sedimentation of nanoparticles, the Van der Waals  
 279 force, and surface charge between the nanoparticles, as well the attractive force  
 280 among the nanoparticles. These forces would help the agglomerations of these

281 nanoparticles, which impact badly on their dispersion in the nanosalt samples.  
282 Therefore, there is a need to find a proper surfactant that could work efficiently at this  
283 high temperature condition, which could help to solve the dispersion and stability  
284 issue of nanoparticles in the nanosalt samples.

285

## 286 **2.2 Latent heat**

287 Latent heat is extensively affected by dispersing nanoparticles into the molten salt.  
288 Particularly, 1 wt. % of  $\text{Fe}_2\text{O}_3$  and CuO in binary salt, 0.5 wt. % of  $\text{Fe}_2\text{O}_3$  and CuO-  
289 single salt, increases the latent heat. The maximum improvement was found within  
290 CuO-binary salt up to 15% and  $\text{Fe}_2\text{O}_3$ -single salt up to 3%. This increment in latent  
291 heat of nanosalt will result with more energy stored per unit volume.

292 An interface is formed during the preparation of nanosalt sample. This interface is  
293 due to the rearrangement of nanoparticles in the nanosalt sample. Therefore,  
294 nanosalt needs higher heat to melt this interfacial layers, which maybe one of the  
295 reasons for increasing latent heat. Additionally, clusters of nanoparticles could lead  
296 to an increase in the latent heat as suggested by Chieruzzi et al. (2015a) and  
297 Lasfargues et al. (2015). More heat is needed to melt these agglomerations.  
298 However, this increasing or decreasing of latent heat of different nanosalts depends  
299 on the places of the presence of nanoparticles in the nanosalt sample. One example  
300 of the current experiments is the increases in latent heat due to the addition of 1 wt.  
301 % CuO nanoparticles into the binary salt. From SEM result Figure (5), it is clearly  
302 shown the agglomerations of 1 wt. % CuO-nanosalt and this sample have a higher  
303 value of latent heat as the clustering required more heat to melt, resulting in an  
304 increment in latent heat. Additionally, as shown in Figure (6) of the samples tested  
305 by SEM results, there is a presence of the agglomerations and clustering of the  
306 nanoparticles in the nanosalt samples. These results are consistent with the  
307 observation from Chieruzzi et al. (2015a) and Lasfargues et al. (2015) for the  
308 enhancements of latent heat of nanosalt samples.

309 Likewise, the melting point of a nanosalt is highly affected by the addition of  
310 nanoparticles in samples.  $T_{\text{melting}}$  is decreased with an addition of nanoparticles in all  
311 cases. In particular, the  $T_{\text{melting}}$  of binary salt is decreased by 5  $^{\circ}\text{C}$  in cases of all  
312 nanosalt samples, i.e  $T_{\text{melting}}$  of binary salt is 230  $^{\circ}\text{C}$  while  $T_{\text{melting}}$  of all the nanosalt is

313 between (225 °C-226 °C). Furthermore, similar behaviour is observed in the case of  
314 KNO<sub>3</sub> base material with a decrement in T<sub>melting</sub> of KNO<sub>3</sub>-nanosalt samples by 1 °C.  
315 This is similar to the results from Gimenez-Gavarrell et al. (2015), Chieruzzi et al.  
316 (2013), Lasfargues et al. (2015) and Chieruzzi et al. (2015a). According to  
317 Lasfargues et al. (2015), T<sub>melting</sub> decrease in nanosalt relies on the method of heat  
318 transfer over nanosalt sample and the size of clustering of these nanoparticles.  
319 Moreover, nanoparticles in the sample could work as nucleation agents, which bring  
320 the phase change earlier in comparison with the base salt, (Gimenez-Gavarrell et al.,  
321 2015). Although this decrement in melting temperature is low, it still considers an  
322 advantage because it means the phase change starts earlier. As a result, melting  
323 time will reduce which improves the heat transfer in the storage system with the  
324 support of enhanced conduction by nanoparticles.

325 Furthermore, the base material in case of binary salt does not reach the eutectic  
326 point as the melting temperature happened in a range of temperature not in a single  
327 point. Because of this, the mixture binary salt behaves as a non-pure mixture  
328 showing that it needs more heat to be melted or freezing completely. According to  
329 Kramer and Wilson (1980), the addition of 60% molar ratio of NaNO<sub>3</sub> would result in  
330 a melting temperature of the binary salt in a temperature range 221 °C > T<sub>melt</sub> > 241  
331 °C. On the other hand, KNO<sub>3</sub> with a composition of 100% have one value for the T<sub>melt</sub>  
332 335 °C as it is a pure single material (Kramer and Wilson, 1980), Figure (7).  
333 However, KNO<sub>3</sub> material used in this experiment was 98% pure. From the DSC  
334 measurements, T<sub>melting</sub> of KNO<sub>3</sub> was in a range caused by its non-purity. The purity of  
335 the material has an impact that influence the behaviour of the salt and nanosalt  
336 properties.

### 337 **3.3 Total thermal energy storage (TES)**

338 TES is the total amount of energy of the storage system by considering both sensible  
339 and latent heats. TES of the nanosalt samples is different from the TES of molten  
340 salt alone. There is an increase or decrease in the TES as shown in Tables (5 and  
341 6). From Table (5), 1 wt.% of Fe<sub>2</sub>O<sub>3</sub>.binary salt and 0.5 wt.% of CuO.binary salt  
342 represent the maximum increment in TES this is due to accumulated increment of  
343 energy. For instance, 1 wt.% of Fe<sub>2</sub>O<sub>3</sub>.binary salt own a higher increase in latent heat  
344 than other concentrations alongside with the advantages of sensible increment in

345 both solid and liquid phases. Although, 1 wt.% of CuO.binary salt gave the maximum  
 346 increases in latent heat, it owns less increment in the sensible heat in comparison to  
 347 the 0.5 wt.%. Therefore, 0.5 wt. % of CuO.binary salt gave a higher TES than that of  
 348 1 wt. % of CuO..

349 It seems to be 0.5 wt. % in single salt (KNO<sub>3</sub>) shows higher increases with 5.26% for  
 350 0.5 wt. % Fe<sub>2</sub>O<sub>3</sub>. KNO<sub>3</sub> as shown in Table (6). TES represents by the summation of  
 351 sensible heat (in the range of working temperatures of solid and liquid phases) and  
 352 of latent heat as shown in the following equations

$$353 \quad q_{storage} = q_{sensible} + q_{latent} \quad (6)$$

$$354 \quad \text{As } q_{sensible} = q_{sensible \text{ in solid phase}} + q_{sensible \text{ in liquid phase}} \quad (7)$$

$$355 \quad q_{storage} = \left[ \int_{T_{ambient}}^{T_{melt}} cp * dT + \int_{T_{liquid}}^{T_{max.}} cp * dT \right] + q_{latent} \quad (8)$$

356

357 In order to increase the storage capacity of the molten salt, an improvement in the  
 358 thermal properties of the molten salt is required. Therefore adding nanoparticles to  
 359 the base material (molten salt) indicated an increase in the sensible/latent storage.  
 360 Most of the cases, nanosalt will have a higher cp and higher latent heat than the  
 361 base material (molten salt) and this leading to a higher efficiency of the storage  
 362 system, which indicated a higher level of the solar thermal power plant efficiency.  
 363 According to Feldhoff et al. (2012), 9 hour is the storage time inside a two tank (hot  
 364 and cold sensible tanks) in the solar thermal plant. The working temperature in the  
 365 cold and hot tanks are 292 °C and 386 °C respectively. Dispersing nanoparticles into  
 366 the base material will improve the c<sub>p</sub> of the base material. 14% is the efficiency of  
 367 TES using molten salt alone, (Feldhoff et al., 2012), while with nanosalt as a storage  
 368 medium this efficiency will increases. For instance, at T= 386 °C, sensible heat of  
 369 solar salt is 220.744 J/kg. However, this sensible heat (220.744 J/kg) can be  
 370 increased when dispersing 1.5 wt. % of CuO in solar salt to 233.044 J/kg. As a  
 371 result, the sensible heat of the nano-binary salt increased by 5.6% in comparison to  
 372 solar salt only, which mean increasing the efficiency of the TES system.  
 373 Furthermore, at T=386 °C, the value of c<sub>p</sub> of nanosalt (KNO<sub>3</sub>+ 1 wt. % Fe<sub>2</sub>O<sub>3</sub>) equals  
 374 to 1.253 J/kg. °C while c<sub>p</sub> of molten salt (KNO<sub>3</sub>) = 1.1615 J/kg. °C. Therefore the

375 sensible heat increased by 7.88% with the presence of nanoparticles. This indicates  
376 the big impact of nanoparticles on the efficiency of the storage system.

377

### 378 **3.4 Thermal conductivity**

379 On the other hand, thermal conductivity ( $k$ ) of binary solar salt,  $\text{Fe}_2\text{O}_3$ -nanosalt, and  
380  $\text{CuO}$ -nanosalt were tested. The current results demonstrate that nanoparticles have  
381 a significant effect on the thermal conductivity of nanosalts both at low and high  
382 temperatures. Increasing concentration of  $\text{CuO}$ , from 0.5 wt. % to 1.5 wt. %, has a  
383 negative effect on thermal conductivity of nanosalt. In contrast,  $\text{Fe}_2\text{O}_3$  nanoparticles  
384 always increase  $k$  of nanosalt except for the case 1 wt. %  $\text{Fe}_2\text{O}_3$ -nanosalt. It is  
385 concluded that small concentrations of nanoparticles are preferred for increasing  $k$  of  
386 nanosalt samples.

387 The increase in temperature leads to an increase in Brownian motion of particles and  
388 this may lead to the enhancement observed in  $k$ . Additionally, these nanoparticles  
389 have higher  $k$  values in comparison with the base salt and therefore when the  
390 nanoparticle is mixed with base salt it would lead to a high  $k$ . However, this  
391 increment in  $k$  of nanosalt depends on the additive material properties, such as  
392 concentration and the type of nanoparticles. For instance, the sample prepared by  
393 the mixing of base salt and the additive material ( $\text{Fe}_2\text{O}_3$ ) seems to be more  
394 conductive material than  $\text{CuO}$ -nanosalt ones as shown in Figure (8). This show the  
395 effect of nanoparticles types on the nanosalt samples. Moreover, the higher surface  
396 area of nanoparticles could be one of the reasons that causes an increases in  
397 thermal conductivity for the nanosalt samples. In addition,  $\text{Fe}_2\text{O}_3$  nanoparticles have  
398 less particle size means higher surface area than  $\text{CuO}$  nanoparticles and this could  
399 be one of the reasons behind the high improvements in  $\text{Fe}_2\text{O}_3$ -nanosalt than  $\text{CuO}$ -  
400 nanosalt samples (Yoo et al., 2007). According to Hwang et al. (2006),  $k$  of nanofluid  
401 is affected by the conductivity of both base and additive materials, which could be  
402 the same case for the current results as both nanoparticles used here have higher  
403 conductivity than a thermal conductivity of molten salt. The improvements in  $k$  of  
404 nanosalt are largely affected by particles loading, the temperature range of the test,  
405 nanoparticles size and stability of the sample. The results of thermal conductivity are  
406 listed in Table (7).



407 Additionally, both nanoparticles (CuO or Fe<sub>2</sub>O<sub>3</sub>) almost show that the lowest  
408 concentration (0.5 wt. %) give more increment in thermal conductivity than higher  
409 concentrations (1 wt. % or 1.5 wt. %). Although, 1.5 wt. % Fe<sub>2</sub>O<sub>3</sub>-nanosalt give better  
410 enhancement than 1 wt. % Fe<sub>2</sub>O<sub>3</sub>-nanosalt case. As shown in Table (7), there is a  
411 maximum increment of nanosalt (in 0.5 wt. %) over the range of concentrations  
412 tested. Figure (9) shows the effect of weight fraction of nanoparticles on thermal  
413 conductivity.

414 In general, k of nanofluids increases with increasing the concentration of  
415 nanoparticle (Mintsa et al., 2009). However, Figure (9) does show a certain  
416 discrepancy as the results for 0.5 wt. % nanosalt is slightly above others  
417 concentrations. According to (Saidur et al., 2011), conductivity increases with  
418 particles loading. This has some differences with current work due to the effect of the  
419 base material. Molten salt behaves differently than water, in addition, the effect of the  
420 surface charge of molten salt could play an important role on the result of k-Temp  
421 result. Furthermore, Assael et al. (2005) mentioned that increases concentrations  
422 from 0.1 to 6 mass % give a decreasing in k by 0.3% to 5% in respective. This is in  
423 matching with the results we got as an increment in particle loading give a lower k.  
424 Although we tested Fe<sub>2</sub>O<sub>3</sub>-nanosalt and CuO-nanosalt, which are different from the  
425 material tested by Assael et al. (2005), their material was carbon nanotube-water  
426 based material. It indicates the big effect of the concentration on the improvement of  
427 k of nanosalt. More work needs to be considered in order to measure k of nanosalt  
428 over a wide range of concentrations to compare the effect of k with nanoparticles'  
429 loading in the nanosalt samples.

430 In order to calculate thermal conductivity theoretically, we would like to consider the  
431 Hamilton-Crosser model as shown in Table (9). According to Hamilton-Crosser  
432 model, the predicted value of k is not matching the measurement values. There are  
433 some reasons that could cause this difference. One of these reasons is the  
434 assumption of the sample in theoretical part compared to the actual behaviour of  
435 sample during the experiments, as the equation assumed the same size of  
436 nanoparticles are dispersed homogeneously along the sample, whereas in the  
437 experiment, it is very difficult to achieve due to the agglomeration and sedimentation  
438 effects of nanoparticles in the nanosalt sample. This could be due to the effects of  
439 different forces such as Van der Waals and gravity forces as both could lead to

440 sedimentation or agglomerations of nanoparticles. Therefore, the calculated values  
441 cannot predict the enhancement in k unless consideration is given to all the affected  
442 factors.

443 Furthermore, the heat transfer will be improved in case of nanosalt due to the  
444 advantages of both  $c_p$ , thermal conductivity. Due to the effect of natural convection  
445 during the phase change any increase in specific heat capacity or thermal  
446 conductivity will causes an increase in the heat transfer rate according to Equation  
447 (9). From heat transfer correlation equation, Nusselt number (Nu) is related to  
448 Rayleigh number (Ra) with some correlations constants, e.g. ( $Nu=CRa^n$ ) as C and n  
449 are constant depending on the case. In addition, any increases in the Nu will causes  
450 an increment in the heat transfer coefficient according to ( $h=Nu*k/L$ ) where h is heat  
451 transfer coefficient, L is the characteristic length and k is thermal conductivity.  
452 Therefore, any increases in Nu will give a higher heat transfer.

$$453 \quad Ra = \frac{g \rho^2 \beta \Delta T L_c}{\mu} * c_p * k \quad (9)$$

454

### 455 **3.5 Comparison with other results**

456 In order to check the accuracy of our results data and to see how much the data we  
457 got are reliable, a comparison was carried out with the literature data.

458 Specific heat capacity and latent heat of molten salt and nanosalt samples have  
459 been compared with other experiments literature data. The average value of  $c_p$  of the  
460  $KNO_3$  salt in Chieruzzi et al. (2015b) was reported to be (1.118 J/g.  $^{\circ}C$ ) and in the  
461 current work is (1.19 J/g.  $^{\circ}C$ ) in the liquid phase. The average value of  $c_p$  of the  
462 binary solar salt ( $NaNO_3:KNO_3$  with 60:40 molar ratio) for the liquid phase equals to  
463 1.315 J/g.  $^{\circ}K$  in the range 250  $^{\circ}C$  -495  $^{\circ}C$  (Jung and Banerjee, 2011) and  $c_p$  has a  
464 value equals to 1.38 J/g.  $^{\circ}K$  in the range 250  $^{\circ}C$ - 450  $^{\circ}C$  by the work of (Xie et al.,  
465 2016). In the current work,  $c_p$  of the binary solar salt for the liquid phase equals to  
466 1.37 J/g. K in the range 250  $^{\circ}C$  -450  $^{\circ}C$ .

467 In order to compare the latent heat values of the current study, first of all,  $KNO_3$  salt  
468 has 91.61 J/g and  $T_{onset}$  is 335.7  $^{\circ}C$  according to Chieruzzi et al. (2015b), in  
469 similarity, the current study  $KNO_3$  salt has a value equals to 93.89 J/g with  $T_{onset}$  is

470 332.47 °C. Secondly, in the current study, the latent heat of solar salt equals to  
471 107.03 J/g with  $T_{\text{onset}}$  is 219.11 °C likely to 110.01 J/g and  $T_{\text{onset}}$  is 219.88 °C by  
472 (Chieruzzi et al., 2013). The standard error of the DSC device used for this  
473 experiments is around 1% and each sample tested for three times and they show a  
474 repeatable and coincide results. However, the small different in the results between  
475 the literature and the current work are more related to the precision of the device  
476 used and the thermal cycle of the test along with the samples used (each salt  
477 purchased from different sources in literature papers and the current work) and the  
478 types of crucible used in DSC device may cause this little differences.

479 Additionally, the thermal conductivity of nitrate salt has been reported by (Serrano-  
480 López et al., 2013). At a range of temperature 250 °C- 400 °C, the difference  
481 between current experiment values and the literature seems to be acceptable in term  
482 of different method used to the measurements as shown in Figure (11).

483 According to Serrano-López et al. (2013), none of the cited literature has mentioned  
484 laser-flash analysis as a measurement device for thermal conductivity of molten  
485 salts. The methods were used for the measurements are transient hot wire, coaxial  
486 cylinder, rough hard sphere, etc. In our experiment, laser-flash analysis have been  
487 used to measure thermal diffusivity of the samples and with the input of known  
488 values of density (based on the literature) and  $c_p$  (based on our experiments), the  
489 thermal conductivity has been calculated, which is approximately matching with the  
490 reported values.

491

#### 492 **4. Conclusion**

493 The specific heat capacity,  $T_{\text{melting}}$ , latent heat and thermal conductivity of nitrate  
494 molten salt were studied using differential scanning calorimetry and laser-flash  
495 analysis, respectively. Different types of nanoparticles (0.5 wt. %, 1 wt. % and 1.5 wt.  
496 %) were dispersed in single salt ( $\text{KNO}_3$ ) and binary salt ( $\text{NaNO}_3:\text{KNO}_3$  with 60:40  
497 molar ratio) to achieve good properties. Using  $\text{Fe}_2\text{O}_3$  nanoparticles, we got a higher  
498 improvement of  $c_p$  up to 11% and thermal conductivity up to 60%. In particular, the  
499 latent heat was increased up to 15% with 1 wt. %  $\text{CuO}$ -binary salt. The storage  
500 energy was improved up to 6% with  $\text{Fe}_2\text{O}_3$  nanoparticles in comparison to solar salt

501 only, which mean an increase of the efficiency of the TES system. Moreover, an  
502 increase in the sensible energy of nano-KNO<sub>3</sub> by 7.88% was observed.

503 In summary, the use of nanosalt to store thermal energy in term of  
504 charging/discharging processes will be very helpful due to their positive effects on  
505 both thermal conductivity and heat capacity.

506

507 **Acknowledgments** Afrah Awad would like to express her gratitude to the high  
508 committee of education development in Iraq (HCED) for the financial support.

509

## 510 **References**

511 ANDREU-CABEDO, P., MONDRAGON, R., HERNANDEZ, L., MARTINEZ-  
512 CUENCA, R., CABEDO, L. & JULIA, J. E. 2014. Increment of specific heat  
513 capacity of solar salt with SiO<sub>2</sub> nanoparticles. *Nanoscale research letters*, 9,  
514 582.

515 ASSAEL, M., METAXA, I., ARVANITIDIS, J., CHRISTOFILOS, D. & LIOUTAS, C.  
516 2005. Thermal conductivity enhancement in aqueous suspensions of carbon  
517 multi-walled and double-walled nanotubes in the presence of two different  
518 dispersants. *International Journal of Thermophysics*, 26, 647-664.

519 BUONGIORNO, J., VENERUS, D. C., PRABHAT, N., MCKRELL, T., TOWNSEND,  
520 J., CHRISTIANSON, R., TOLMACHEV, Y. V., KEBLINSKI, P., HU, L.-W. &  
521 ALVARADO, J. L. 2009. A benchmark study on the thermal conductivity of  
522 nanofluids. *Journal of Applied Physics*, 106, 094312.

523 CHIERUZZI, M., CERRITELLI, G. F., MILIOZZI, A. & KENNY, J. M. 2013. Effect of  
524 nanoparticles on heat capacity of nanofluids based on molten salts as PCM  
525 for thermal energy storage. *Nanoscale research letters*, 8, 448.

526 CHIERUZZI, M., CERRITELLI, G. F., MILIOZZI, A., KENNY, J. M. & TORRE, L.  
527 2017. Heat capacity of nanofluids for solar energy storage produced by  
528 dispersing oxide nanoparticles in nitrate salt mixture directly at high  
529 temperature. *Solar Energy Materials and Solar Cells*, 167, 60-69.

530 CHIERUZZI, M., MILIOZZI, A., CRESCENZI, T., TORRE, L. & KENNY, J. M. 2015a.  
531 A new phase change material based on potassium nitrate with silica and

532 alumina nanoparticles for thermal energy storage. *Nanoscale research letters*,  
533 10, 273.

534 CHIERUZZI, M., MILIOZZI, A., CRESCENZI, T., TORRE, L. & KENNY, J. M. 2015b.  
535 A new phase change material based on potassium nitrate with silica and  
536 alumina nanoparticles for thermal energy storage. *Nanoscale research letters*,  
537 10, 1.

538 CHOL, S. 1995. Enhancing thermal conductivity of fluids with nanoparticles. *ASME-*  
539 *Publications-Fed*, 231, 99-106.

540 DUDDA, B. & SHIN, D. 2013. Effect of nanoparticle dispersion on specific heat  
541 capacity of a binary nitrate salt eutectic for concentrated solar power  
542 applications. *International journal of thermal sciences*, 69, 37-42.

543 FELDHOFF, J. F., SCHMITZ, K., ECK, M., SCHNATBAUM-LAUMANN, L., LAING,  
544 D., ORTIZ-VIVES, F. & SCHULTE-FISCHEDICK, J. 2012. Comparative  
545 system analysis of direct steam generation and synthetic oil parabolic trough  
546 power plants with integrated thermal storage. *Solar Energy*, 86, 520-530.

547 GIMENEZ-GAVARRELL, P., ROMANIN, V. D. & FERERES, S. Latent Heat of  
548 Fusion and Melting Temperature of Molten Salt Based Carbon Nanotube  
549 Suspensions Used as Phase Change Materials. ASME 2015 9th International  
550 Conference on Energy Sustainability collocated with the ASME 2015 Power  
551 Conference, the ASME 2015 13th International Conference on Fuel Cell  
552 Science, Engineering and Technology, and the ASME 2015 Nuclear Forum,  
553 2015. American Society of Mechanical Engineers, V001T10A005-  
554 V001T10A005.

555 HWANG, Y., AHN, Y., SHIN, H., LEE, C., KIM, G., PARK, H. & LEE, J. 2006.  
556 Investigation on characteristics of thermal conductivity enhancement of  
557 nanofluids. *Current Applied Physics*, 6, 1068-1071.

558 JANZ, G., KREBS, U., SIEGENTHALER, H. & TOMKINS, R. 1972. Molten salts:  
559 Volume 3 nitrates, nitrites, and mixtures: Electrical conductance, density,  
560 viscosity, and surface tension data. *Journal of Physical and Chemical*  
561 *Reference Data*, 1, 581-746.

562 JUNG, S. & BANERJEE, D. 2011. Enhancement of heat capacity of nitrate salts  
563 using mica nanoparticles. *Dev Strateg Mater Comput Des II: Ceram Eng Sci*  
564 *Proc*, 32, 127-137.

565 KONG, L. B., LI, T., HNG, H. H., BOEY, F., ZHANG, T. & LI, S. 2014. Waste Energy  
566 Harvesting. *Springer, New York*.

567 KRAMER, C. M. & WILSON, C. J. 1980. The phase diagram of NaNO<sub>3</sub>—KNO<sub>3</sub>.  
568 *Thermochimica Acta*, 42, 253-264.

569 LAING, D., BAUER, T., STEINMANN, W.-D. & LEHMANN, D. 2009. Advanced high  
570 temperature latent heat storage system-design and test results. *Effstock*  
571 *2009, Abstract Book and Proceedings*.

572 LASFARGUES, M., GENG, Q., CAO, H. & DING, Y. 2015. Mechanical dispersion of  
573 nanoparticles and its effect on the specific heat capacity of impure binary  
574 nitrate salt mixtures. *Nanomaterials*, 5, 1136-1146.

575 LU, M.-C. & HUANG, C.-H. 2013. Specific heat capacity of molten salt-based  
576 alumina nanofluid. *Nanoscale research letters*, 8, 292.

577 LUO, Y., DU, X., AWAD, A. & WEN, D. 2017. Thermal energy storage enhancement  
578 of a binary molten salt via in-situ produced nanoparticles. *International Journal*  
579 *of Heat and Mass Transfer*, 104, 658-664.

580 MINTSA, H. A., ROY, G., NGUYEN, C. T. & DOUCET, D. 2009. New temperature  
581 dependent thermal conductivity data for water-based nanofluids. *International*  
582 *Journal of Thermal Sciences*, 48, 363-371.

583 MYERS, P. D., ALAM, T. E., KAMAL, R., GOSWAMI, D. & STEFANAKOS, E. 2016.  
584 Nitrate salts doped with CuO nanoparticles for thermal energy storage with  
585 improved heat transfer. *Applied Energy*, 165, 225-233.

586 NETZSCH 2017. PART A - Theoretical background, LFA 427, Operating  
587 Instructions, 09.93. 1-32.

588 NIU, D., LU, Y. & WU, D. 2014. Development of a novel thermal storage molten-salt  
589 filled with nanoparticles for concentration solar plants. *Bulgarian Chemical*  
590 *Communications*, 46.

591 PFLEGER, N., BAUER, T., MARTIN, C., ECK, M. & WÖRNER, A. 2015. Thermal  
592 energy storage—overview and specific insight into nitrate salts for sensible and  
593 latent heat storage. *Beilstein journal of nanotechnology*, 6, 1487.

594 RIAZI, H., MESGARI, S., AHMED, N. A. & TAYLOR, R. A. 2016. The effect of  
595 nanoparticle morphology on the specific heat of nanosalts. *International*  
596 *Journal of Heat and Mass Transfer*, 94, 254-261.

597 SAIDUR, R., LEONG, K. Y. & MOHAMMAD, H. A. 2011. A review on applications  
598 and challenges of nanofluids. *Renewable and Sustainable Energy Reviews*,  
599 15, 1646-1668.

600 SCHULLER, M., LITTLE, F., MALIK, D., BETTS, M., SHAO, Q., LUO, J., ZHONG,  
601 W., SHANKAR, S. & PADMANABAN, A. 2012. Molten Salt-Carbon Nanotube  
602 Thermal Energy Storage for Concentrating Solar Power Systems Final  
603 Report. Texas Engineering Experiment Station.

604 SCHULLER, M., SHAO, Q. & LALK, T. 2015. Experimental investigation of the  
605 specific heat of a nitrate–alumina nanofluid for solar thermal energy storage  
606 systems. *International Journal of Thermal Sciences*, 91, 142-145.

607 SERRANO-LÓPEZ, R., FRADERA, J. & CUESTA-LÓPEZ, S. 2013. Molten salts  
608 database for energy applications. *Chemical Engineering and Processing:  
609 Process Intensification*, 73, 87-102.

610 SHIN, D. 2011. *Molten salt nanomaterials for thermal energy storage and  
611 concentrated solar power applications*. Texas A&M University.

612 SNOW, C. L., LEE, C. R., SHI, Q., BOERIO-GOATES, J. & WOODFIELD, B. F.  
613 2010. Size-dependence of the heat capacity and thermodynamic properties of  
614 hematite ( $\alpha$ -Fe<sub>2</sub>O<sub>3</sub>). *The Journal of Chemical Thermodynamics*, 42, 1142-  
615 1151.

616 THIRUGNANASAMBANDAM, M., INIYAN, S. & GOIC, R. 2010. A review of solar  
617 thermal technologies. *Renewable and sustainable energy reviews*, 14, 312-  
618 322.

619 VAJJHA, R., DAS, D. & MAHAGAONKAR, B. 2009. Density measurement of  
620 different nanofluids and their comparison with theory. *Petroleum Science and  
621 Technology*, 27, 612-624.

622 XIE, Q., ZHU, Q. & LI, Y. 2016. Thermal Storage Properties of Molten Nitrate Salt-  
623 Based Nanofluids with Graphene Nanoplatelets. *Nanoscale Research Letters*,  
624 11, 1-7.

625 YOO, D.-H., HONG, K. & YANG, H.-S. 2007. Study of thermal conductivity of  
626 nanofluids for the application of heat transfer fluids. *Thermochimica Acta*, 455,  
627 66-69.

628

629

## Tables and Figures

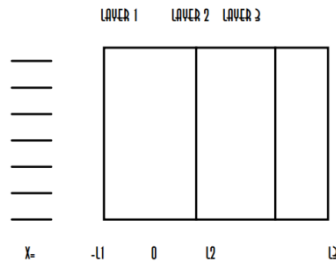


Figure 1 three layer model (NETZSCH, 2017)

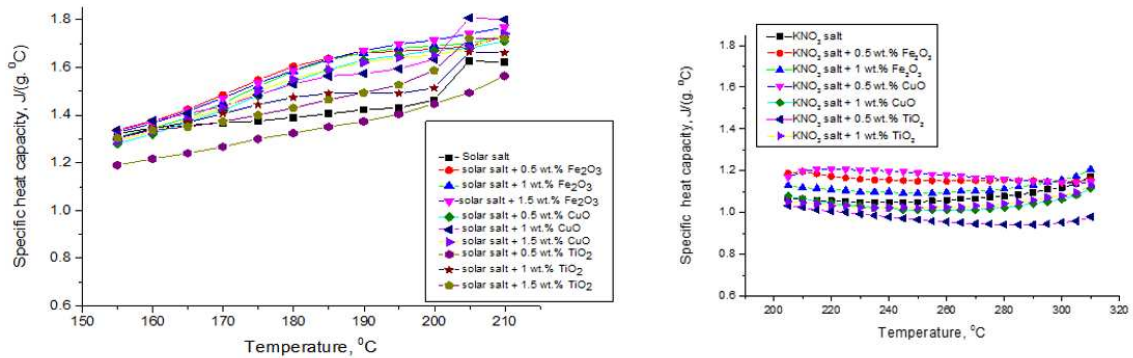


Figure 2 Solid phase of cp of different types and concentrations of nanoparticles dispersed into nitrate salt.

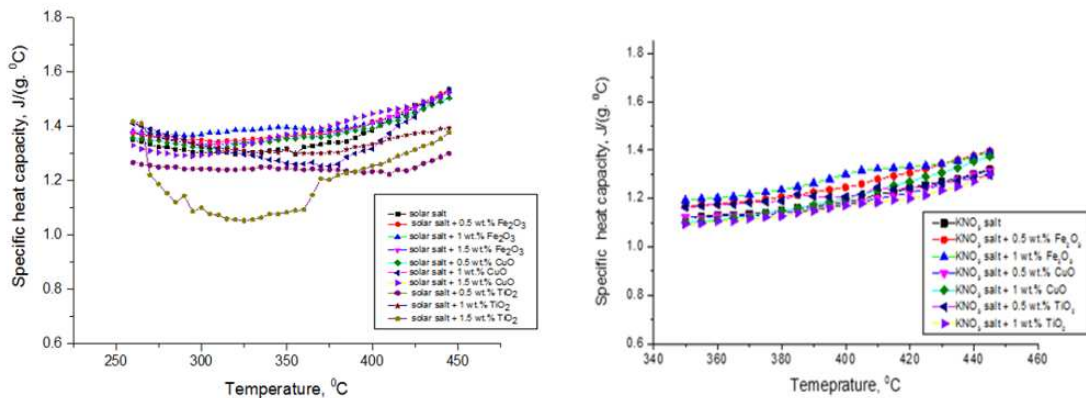
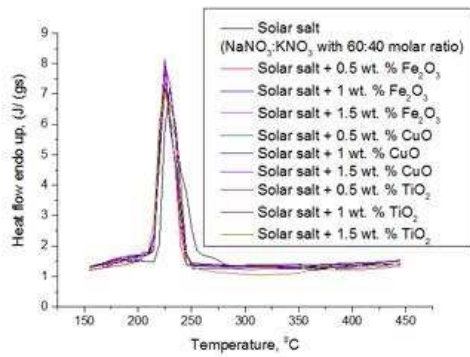


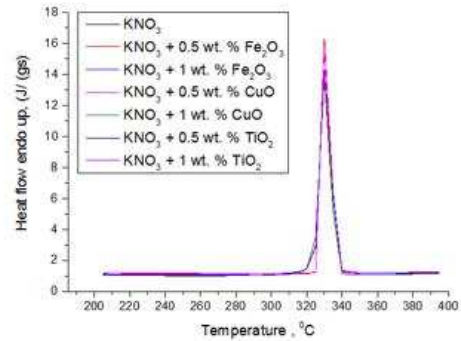
Figure 3 Specific heat capacity of liquid phase of different types and concentrations of nanoparticles dispersed in nitrate salt



655  
656  
657  
658  
659  
660  
661  
662  
663  
664  
665  
666  
667  
668  
669  
670  
671  
672  
673  
674  
675  
676  
677  
678



Heat flow vs. temperature of binary salt and nanosalts



Heat flow vs. temperature of KNO<sub>3</sub> and nanosalts

**Figure 4 Heat flow vs. temperature of salt and nanosalts**

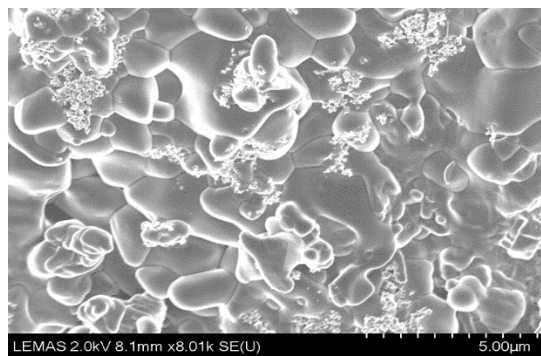
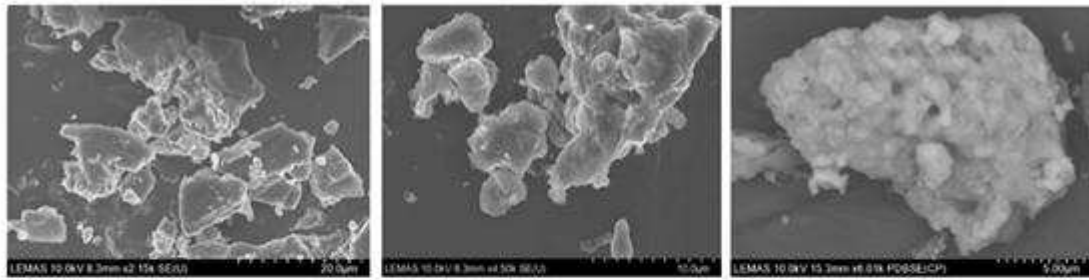
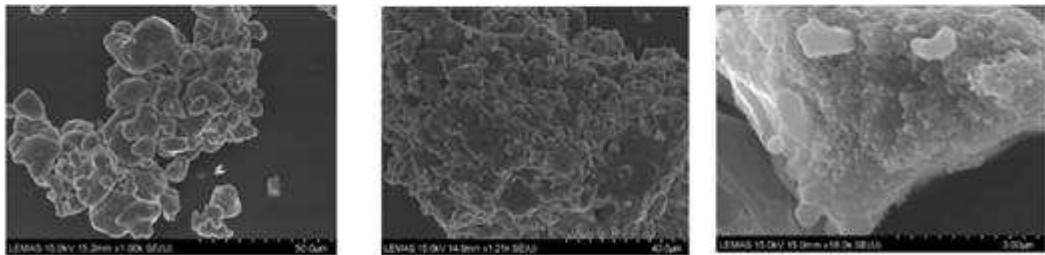


**Figure 5 SEM test of 1 wt. % CuO dispersed in solar salt.**

679  
680  
681  
682  
683  
684  
685  
686  
687  
688  
689  
690  
691  
692  
693  
694  
695  
696  
697  
698  
699  
700  
701  
702



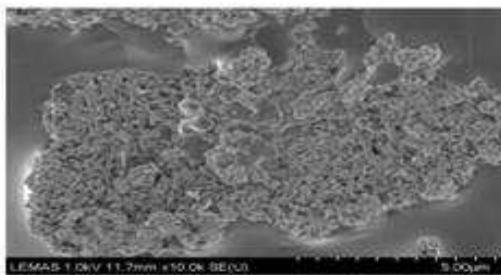
1 wt. % Fe<sub>2</sub>O<sub>3</sub> dispersed in solar salt.



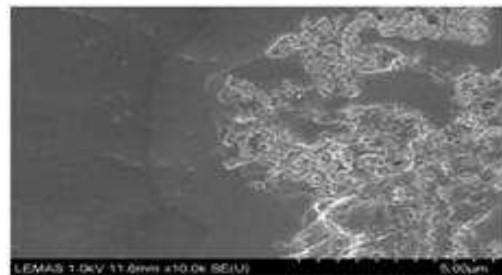
1 wt. % Fe<sub>2</sub>O<sub>3</sub> dispersed in KNO<sub>3</sub> salt.

0.5 wt. % CuO dispersed in solar salt

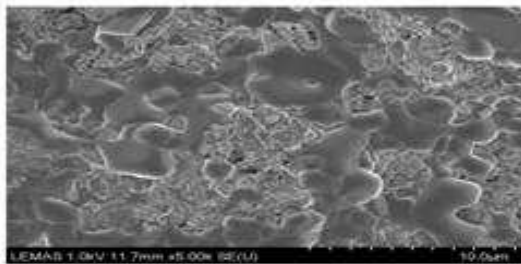
0.5 wt. % CuO dispersed in KNO<sub>3</sub> salt.



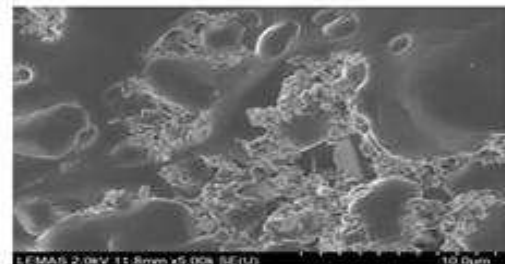
0.5 wt. % Fe<sub>2</sub>O<sub>3</sub> dispersed in KNO<sub>3</sub> after melting/solidification cycles



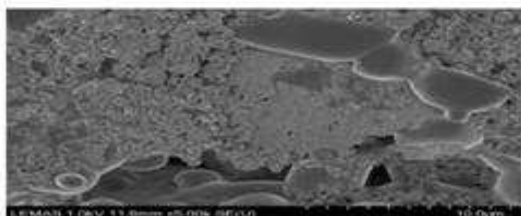
0.5 wt. % TiO<sub>2</sub> dispersed in KNO<sub>3</sub> after melting/solidification cycles



0.5 wt. % CuO dispersed in solar salt after melting/solidification



0.5 wt. % Fe<sub>2</sub>O<sub>3</sub> dispersed in solar salt after melting/solidification



1 wt. % Fe<sub>2</sub>O<sub>3</sub> dispersed in solar salt after melting/solidification



1 wt. % TiO<sub>2</sub> dispersed in solar salt after melting/solidification

Figure 6 SEM shows nanoparticle agglomerations after the preparation

703  
704  
705  
706  
707  
708  
709  
710  
711  
712  
713  
714  
715  
716  
717  
718  
719  
720  
721  
722  
723  
724  
725  
726  
727

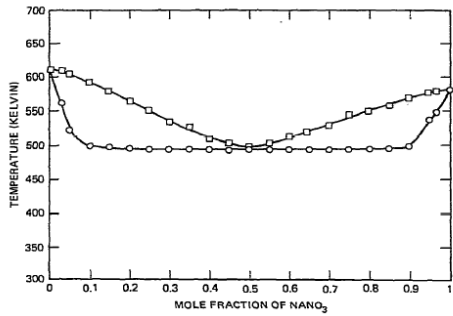


Figure 7 phase diagram of solar salt with different composition of NaNO<sub>3</sub> (Kramer and Wilson, 1980)

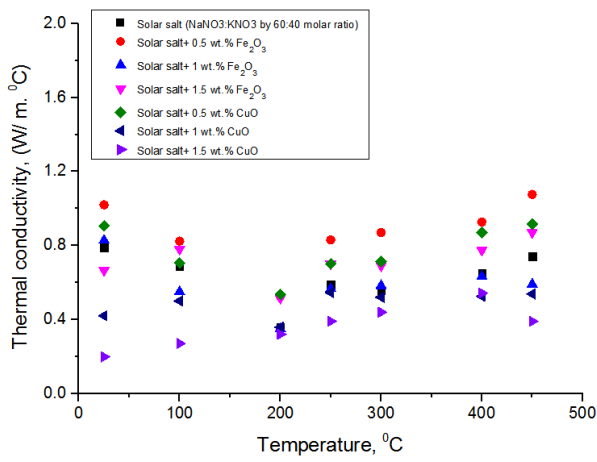


Figure 8 thermal conductivity vs. temperature of different samples.

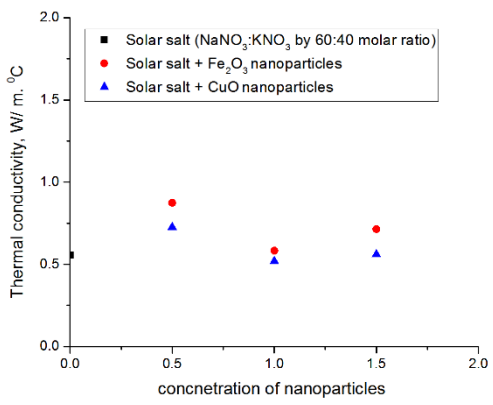
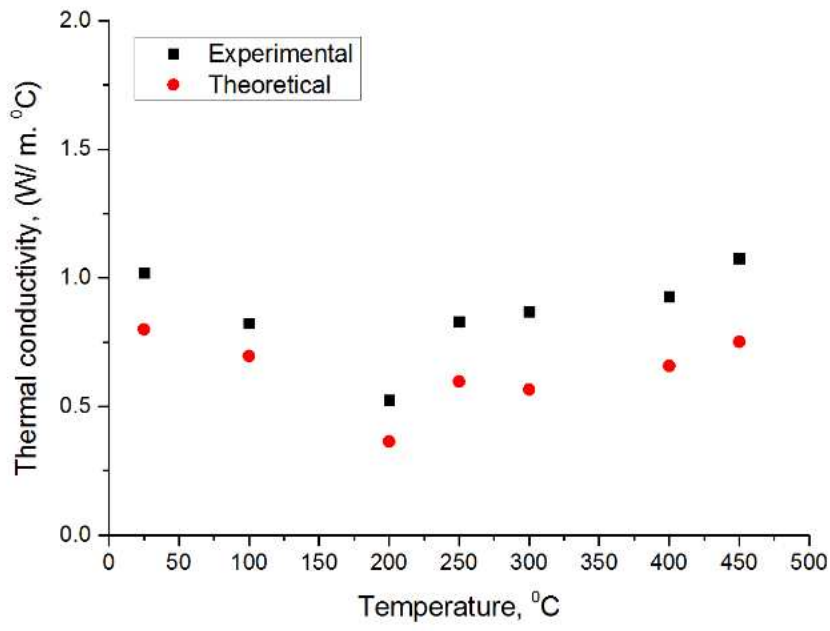
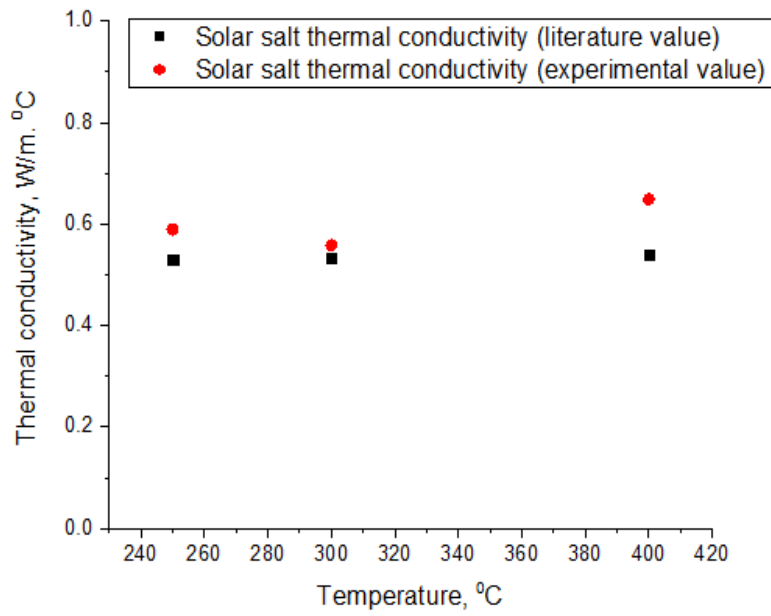


Figure 9 Thermal conductivity of nanosalt vs concentration of nanoparticles

728  
729  
730  
731  
732  
733  
734  
735  
736  
737  
738  
739  
740  
741  
742  
743  
744  
745  
746  
747  
748  
749  
750  
751  
752  
753

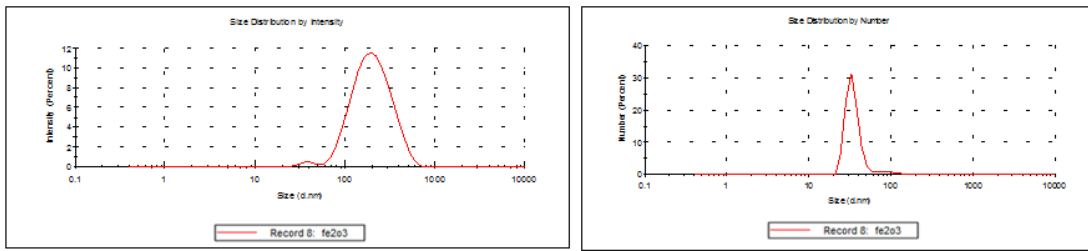


**Figure 10 thermal conductivity vs temperature for 0.5 wt. % Fe<sub>2</sub>O<sub>3</sub>-nanosalt both experimental and calculated values**



**Figure 111 thermal conductivity of current experiment and in the literature (Serrano-López et al., 2013)**

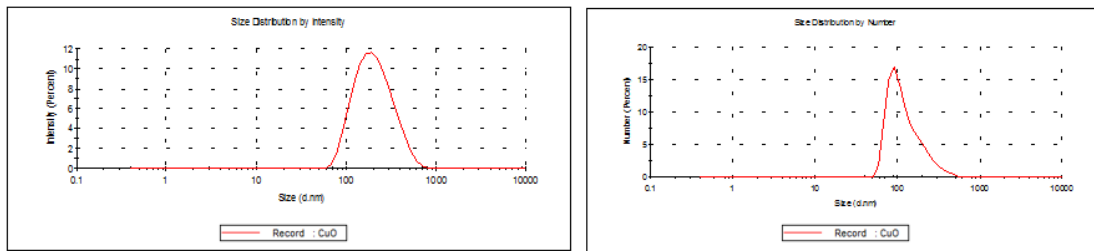
754  
755  
756  
757  
758  
759



Fe<sub>2</sub>O<sub>3</sub>-nanofluid with average size of (175.5 nm)

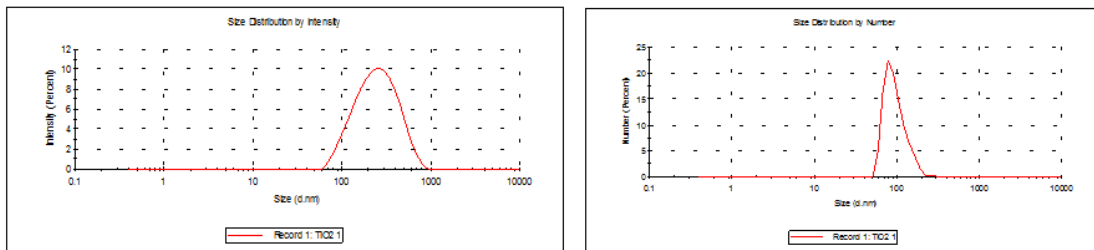
760

763  
764  
765



CuO-nanofluid with average size of (182.5 nm)

766  
767  
768  
769  
770  
771



TiO<sub>2</sub>-nanofluid with average size of (214 nm)

772  
773 **Figure 122 Size measurement in DLS device for different nanofluid samples.**

774  
775  
776

777

778 **Table 1 Solid phase of cp (in range 150 °C-215 °C) of different types and concentrations**  
 779 **of nanoparticles dispersed inside solar salt (NaNO<sub>3</sub>:KNO<sub>3</sub> by 60:40 molar ratios).**

Run	Solar salt	+ Fe <sub>2</sub> O <sub>3</sub>			+ CuO			+ TiO <sub>2</sub>		
	-	0.5 wt.%	1 wt.%	1.5 wt.%	0.5 wt.%	1 wt.%	1.5 wt.%	0.5 wt.%	1 wt.%	1.5 wt.%
<b>Run 1</b>	1.43	1.67	1.63	1.67	1.59	1.37	1.64	1.27	1.31	1.3
<b>Run 2</b>	1.44	1.49	1.54	1.53	1.48	1.63	1.49	1.41	1.52	1.53
<b>Run 3</b>	1.43	1.54	1.51	1.53	1.51	1.56	1.48	1.36	1.53	1.52
<b>Average</b>	1.43	1.57	1.56	1.58	1.53	1.52	1.54	1.35	1.453	1.45
<b>% Increase</b>	-	9.8%	9.1%	10.5%	7%	6.3%	7.7%	-5.6%	1.6%	1.4%

780

781 **Table 2 Solid phase of cp (in range 200 °C-315 °C) of different types and concentrations**  
 782 **of nanoparticles dispersed into KNO<sub>3</sub> salt.**

Run	KNO <sub>3</sub> salt	+ Fe <sub>2</sub> O <sub>3</sub>		+ CuO		+ TiO <sub>2</sub>	
	-	0.5 wt.%	1 wt.%	0.5 wt.%	1 wt.%	0.5 wt.%	1 wt.%
<b>Run 1</b>	1.09	1.17	1.12	1.16	1.06	0.78	1.06
<b>Run 2</b>	1.072	1.15	1.11	1.151	1.03	1.085	1.04
<b>Run 3</b>	1.073	1.13	1.13	1.150	1.04	1.065	1.039
<b>Average</b>	1.078	1.15	1.12	1.154	1.043	0.98	1.046
<b>% Increase</b>	-	6.68%	3.9%	7.05%	-3.25%	-9.09%	-2.97%

783

784

785 **Table 3 Liquid phase of cp (in range 250 °C-450 °C) of different types and**  
 786 **concentrations of nanoparticles dispersed inside solar salt (NaNO<sub>3</sub>:KNO<sub>3</sub> by 60:40**  
 787 **molar ratios).**

Run	Solar salt	+ Fe <sub>2</sub> O <sub>3</sub>			+ CuO			+ TiO <sub>2</sub>		
	-	0.5 wt.%	1 wt.%	1.5 wt.%	0.5 wt.%	1 wt.%	1.5 wt.%	0.5 wt.%	1 wt.%	1.5 wt.%
<b>Run 1</b>	1.38	1.36	1.33	1.37	1.36	1.37	1.35	1.14	1.27	0.9
<b>Run 2</b>	1.37	1.363	1.46	1.39	1.37	1.34	1.34	1.3	1.35	1.32
<b>Run 3</b>	1.35	1.46	1.42	1.39	1.4	1.32	1.45	1.31	1.39	1.30
<b>Average</b>	1.37	1.394	1.4	1.383	1.377	1.343	1.38	1.25	1.34	1.17
<b>% Increase</b>	-	1.75%	2.19%	0.95%	0.51%	-1.97%	0.73%	-8.76%	-2.19%	-14.6%

788

789

790 **Table 4 Liquid phase of cp (in range 350 °C-390 °C) of different types and**  
 791 **concentrations of nanoparticles dispersed into KNO<sub>3</sub> salt**

Run	KNO <sub>3</sub> salt	+ Fe <sub>2</sub> O <sub>3</sub>		+ CuO		+ TiO <sub>2</sub>	
	-	0.5 wt.%	1 wt.%	0.5 wt.%	1 wt.%	0.5 wt.%	1 wt.%
<b>Run 1</b>	1.18	1.22	1.28	1.21	1.18	1.14	1.171

<b>Run 2</b>	1.2	1.28	1.27	1.18	1.22	1.28	1.17
<b>Run 3</b>	1.2	1.27	1.28	1.17	1.216	1.245	1.16
<b>Average</b>	1.19	1.26	1.28	1.187	1.205	1.222	1.167
<b>% Increase</b>	-	5.9%	7.56%	-0.25%	1.261%	2.69%	-1.93%

792

793

794 **Table 5 latent heat, onset temperature and total thermal energy storage capacity of**  
795 **different types and concentrations of nanoparticles dispersed in solar salt**  
796 **(NaNO<sub>3</sub>:KNO<sub>3</sub> by 60:40 molar ratios).**

Material	Latent heat (kJ/kg)	Onset temperature (°C)	T <sub>onset</sub> differences	Total TES capacity (kJ/kg)	% TES
Pure salt	107.03	219.11	-	466.83	-
Salt + 0.5 wt. % Fe <sub>2</sub> O <sub>3</sub>	109.27	216.22	2.89	482.27	3.31%
Salt + 1 wt. % Fe <sub>2</sub> O <sub>3</sub>	119.09	219	0.11	492.69	5.54%
Salt + 1.5 wt % Fe <sub>2</sub> O <sub>3</sub>	115.25	216.66	2.45	486.65	4.25%
Salt + 0.5 wt % CuO	118.08	216.01	3.1	485.28	3.95%
Salt + 1 wt % CuO	122.5	218.21	0.9	482.3	3.31%
Salt + 1.5 wt % CuO	110.32	217.05	2.06	478.72	2.55%
Salt + 0.5 wt % TiO <sub>2</sub>	95.41	216.33	2.78	426.41	-8.66%
Salt + 1 wt % TiO <sub>2</sub>	100.37	215.88	3.23	455.55	-2.42%
Salt + 1.5 wt % TiO <sub>2</sub>	89.65	213.31	5.8	410.65	-12.03%

797

798

799 **Table 6 latent heat, onset temperature and total thermal energy storage capacity of**  
800 **different types and concentrations of nanoparticles dispersed inside KNO<sub>3</sub> salt.**

Material	Latent heat (kJ/kg)	Onset temperature (°C)	T <sub>onset</sub> differences	Total TES capacity (kJ/kg)	% TES
KNO <sub>3</sub> salt	93.89	332.47	0	331.47	-
KNO <sub>3</sub> salt + 0.5 wt. % Fe <sub>2</sub> O <sub>3</sub>	96.41	332.12	0.35	348.91	5.26%
KNO <sub>3</sub> salt + 1 wt. % Fe <sub>2</sub> O <sub>3</sub>	94.08	325.53	6.94	345.28	4.17%
KNO <sub>3</sub> salt + 0.5 wt % CuO	95.14	332.3	0.17	340.78	2.81%
KNO <sub>3</sub> salt + 1 wt % CuO	94.42	330.78	1.69	329.65	-0.55%
KNO <sub>3</sub> salt+ 0.5 wt % TiO <sub>2</sub>	91.02	327.56	4.91	321.02	-3.15%
KNO <sub>3</sub> salt+ 1 wt % TiO <sub>2</sub>	92.9	325.55	6.92	324.66	-2.05%

801



802  
803

**Table 7 thermal conductivity (k, W/m. C) of different types and concentrations of nanosalt**

T, °C	Molten salt	Molten salt+ 0.5 wt.% Fe <sub>2</sub> O <sub>3</sub>	Molten salt+ 1 wt.% Fe <sub>2</sub> O <sub>3</sub>	Molten salt+ 1.5 wt.% Fe <sub>2</sub> O <sub>3</sub>	Molten salt+ 0.5 wt.% CuO	Molten salt+ 1 wt.% CuO	Molten salt+ 1.5 wt.% CuO
25	0.79	1.02	0.828	0.665	0.906	0.42	0.198
100	0.687	0.823	0.55	0.78	0.705	0.5	0.27
200	0.359	0.524	0.35	0.515	0.536	0.358	0.32
250	0.589	0.83	0.566	0.7	0.701	0.545	0.39
300	0.558	0.87	0.583	0.69	0.713	0.52	0.439
400	0.649	0.927	0.632	0.774	0.87	0.525	0.543
450	0.742	1.076	0.59	0.87	0.915	0.538	0.39

804  
805  
806

**Table 8 Enhancement in thermal conductivity of different types and concentrations of nanosalt**

T, °C	Molten salt+ 0.5 wt.% Fe <sub>2</sub> O <sub>3</sub>	Molten salt+ 1 wt.% Fe <sub>2</sub> O <sub>3</sub>	Molten salt+ 1.5 wt.% Fe <sub>2</sub> O <sub>3</sub>	Molten salt+ 0.5 wt.% CuO	Molten salt+ 1 wt.% CuO	Molten salt+ 1.5 wt.% CuO
25	29.1	4.81	-15.8	14.68	-46.84	-74.94
100	19.8	-19.94	13.54	2.62	-27.22	-60.7
200	45.96	-2.51	43.45	49.3	-0.28	-10.86
250	40.92	-3.9	18.85	19.02	-7.47	-33.79
300	55.91	4.48	23.66	27.78	-6.81	-21.33
400	42.84	-2.62	19.26	34.05	-19.11	-16.33
450	45.01	-20.49	17.25	23.32	-27.49	-47.44

807  
808

**Table 9 theoretical calculations of thermal conductivity for different types and concentrations of nanosalt**

T, °C	Molten salt+ 0.5 wt.% Fe <sub>2</sub> O <sub>3</sub>	Molten salt+ 1 wt.% Fe <sub>2</sub> O <sub>3</sub>	Molten salt+ 1.5 wt.% Fe <sub>2</sub> O <sub>3</sub>	Molten salt+ 0.5 wt.% CuO	Molten salt+ 1 wt.% CuO	Molten salt+ 1.5 wt.% CuO
25	0.8	0.81	0.821	0.802	0.814	0.826
100	0.696	0.705	0.714	0.697	0.708	0.718
200	0.364	0.369	0.374	0.364	0.37	0.375
250	0.597	0.605	0.613	0.598	0.607	0.616
300	0.566	0.573	0.581	0.566	0.575	0.583
400	0.658	0.666	0.675	0.659	0.669	0.679
450	0.752	0.761	0.771	0.753	0.764	0.776

809